AN EXAMINATION OF INTERACTIONS BETWEEN FLUID VISCOUS DAMPERS AND DIAPHRAGMS – DEVELOPING APPROXIMATE METHODS FOR USE WITH LINEAR DESIGN METHODS

Nathan E. Canney, PhD, PE
Taylor Devices Inc.
North Tonawanda, NY

David P. Welch, PhD
Haselton Baker Risk Group
Chico, CA

D. Jared DeBock, PhD, PE
Haselton Baker Risk Group/ CSU Chico
Chico, CA

Abstract

The use of fluid viscous dampers (FVDs) is becoming more common in engineering practice, particularly for retrofit applications and for improved resiliency in new critical facilities like hospitals. Because FVDs are velocity dependent and do not contribute stiffness to the structure, there are unique considerations with respect to the interaction between the force generated by the FVDs and the diaphragm at each floor. In typical practice, Nonlinear Response History Analysis is used in the design and analysis of structures with FVDs and, in these cases, the step-by-step interactions between the dampers, lateral system and inertial forces of the diaphragm are captured. When linear methods are used, as is the case with a newly certified prescriptive method for the design of damped moment frames, the Taylor Damped Moment Frame, there is no guidance on how to navigate these interactions.

This paper explores the interactions between the forces generated by FVDs and diaphragm inertial demands. An expansive archetype design space of steel moment frames with supplemental damping was developed with designs that follow the Taylor Damped Moment Frame prescriptive method in alignment with ICC-ESR 4769. A subset of the archetype space was evaluated in *OpenSees* with a set of 44 ground motions to determine damper forces from the floor above and floor below a given diaphragm at each time step. The interaction of these forces corresponds to the contribution to each diaphragm. Finally, a prescriptive approach to determining the damper-induced demands into a diaphragm for varying conditions is provided. This prescriptive method is rooted in the results from the archetype study and would be useful for schematic level evaluations as well as any design of damped moment frame structures with fluid viscous dampers using linear methods.

Introduction

Fluid Viscous Dampers (FVDs) are an effective way to reduce seismic demands on a structure. Typically, an FVD is connected between two adjacent floors, capitalizing on the differential movement between the floors to drive the FVD back and forth (Figure 1). As the device strokes due to the relative movement of the floors, a piston head inside of the device is forced through a fluid (typically silicone or oil), thereby converting kinetic energy into heat energy which dissipates into the environment. The viscous damping provided by the FVD supplements hysteretic and inherent damping within the

structure, reducing deformation and yielding in the structural system, limits damage to structural and nonstructural components and helps improve structural resilience.

FVDs are velocity-dependent devices governed by the constitutive equation:

$$F = CV^{\alpha} \quad \text{(Eqn. 1)}$$

Where, F is the output force; C is the damping constant; V is the velocity and α is the velocity exponent.

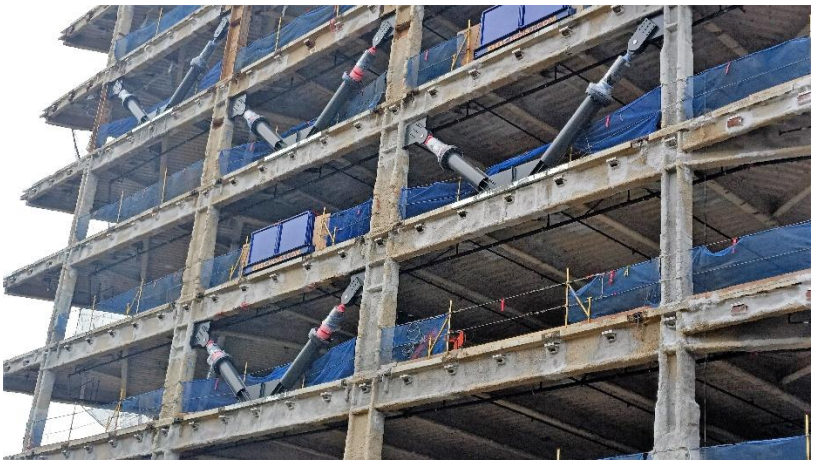

Figure 1. Dampers Placed in Inverted-Chevron Configurations at Multiple Stories

Because FVDs are velocity-dependent devices, nonlinear dynamic analysis is typically required to capture the effects of the FVDs on the behavior of a structure. Most practicing engineers utilize Nonlinear Response History Analysis in the evaluation of damped structures to optimize damper properties and capture the interplay between the velocity-based output force of the dampers with the displacement and acceleration dependent force demands of the Lateral Force Resisting System (LFRS) and associated elements.

Linear procedures, however, have been developed and utilized in the design of structures with FVDs since their early adoption. The Modal Strain Energy method, for example, approximates the ratio of the energy dissipated by the dampers to the strain energy of the elastic structure on a mode-by-mode basis (Ramirez et al., 2001). This approach forms the basis for the linear static and linear dynamic approaches presented in both ASCE 7 and ASCE 41. In this approach, an estimation of the viscous damping ratio is determined and then used to reduce the response spectrum used to determine the seismic base shear (and thereby the story forces and drift).

Furthering the linear approaches in design codes for buildings with dampers, the Taylor Damped Moment Frame™ (TDMF™) was developed as a prescriptive approach for the design of Steel Special Moment Frames (SMFs) with supplemental damping provided by FVDs. Through the ICC-ES AC494 process (ICC-ES, 2019), grounded in analysis utilizing the FEMA P-695 framework (FEMA, 2009), a design procedure was developed and validated. The resulting design procedure was approved by ICC in 2023 and is captured in ICC-ESR 4769 (ICC-ES, 2023) as an Alternative Structural System per ASCE 7-22 Section 12.2.1.1 (ASCE, 2022).

The TDMF™ design procedure is rooted in Modal Response Spectrum Analysis (MRSA) where the Response Modification Coefficient (R) and Deflection Amplification Factor (C_d), along with a specific design procedure, were validated through incremental dynamic analysis (Vamvatsikos and Cornell, 2002) of a suite of archetype structures. Through this process, it was established that structures designed using this prescriptive approach meet the collapse probability intentions of the

building code, namely that Risk Category II structures achieve a collapse probability of 10% or less at the MCE_R level event. Welch et al. (2022) explain this process and summarize results for the TDMF™ system in more detail.

While the TDMF™ prescriptive method details the selection of damper properties, the impact of the dampers on the LFRS system demands and the generalized inclusion of the output damper force back into the system, there is a gap in direction as to how to incorporate the damper-induced lateral force into the diaphragm design. This gap exists in the linear methods of ASCE 7 and ASCE 41 as well. This paper presents results and suggested approaches for the incorporation of the damper-induced forces into a diaphragm for various conditions, applicable when using the TDMF™ design procedure.

Archetype Design Space

This section provides an overview of the archetype designs used for this diaphragm study – a subset of the entire archetype design space used for the ICC-ES AC494 process (See Welch et al., 2022). A standard floor plan for the archetype structures is shown in Figure 2. A total of 51 archetype structures were used for this sub-study. The base structure uses a fixed base condition with a first story height of 16 feet and 14 feet for all other stories. All archetype designs utilized dampers in a chevron configuration where the dampers were placed outside of the moment frame and without any shared elements (a Type I configuration per ICC-ESR 4769). All structures were designed for Seismic Design Category D_{max} (S_{DS} = 1.0, S_{D1} = 0.6) and as Risk Category II structures. A summary of the properties and quantities of the archetype structures used is provided in Table 1; including descriptions of archetype variants that deviate from the base structure.

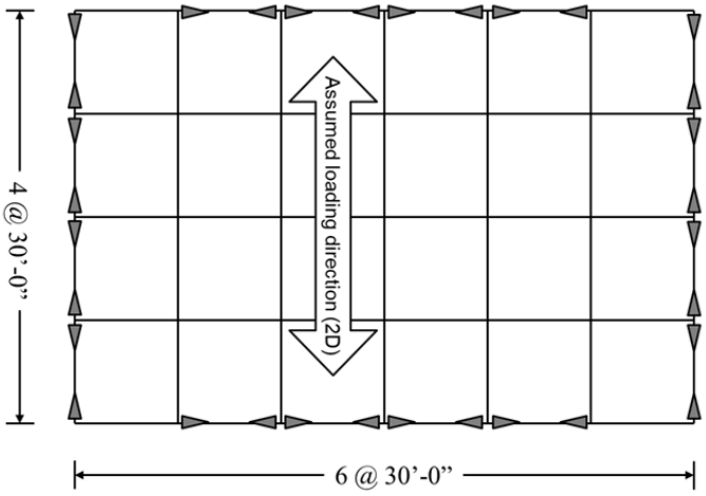

Figure 2. Standard Archetype Floor Plan

Table 1. Archetype Structure Properties and Quantities

Number of Stories (quantity)	MF Connection Type	MF Tributary Gravity*	Upper Limit on MF Column Size	Other Property Variations
2 (5)	RBS w/ Doubler Pl. (3); RBS w/o Doubler Pl. (1); WUF-W (1)	High (0); Low (5);	W12 (5)	Pin-base condition (2); Welded beam-column @ Damper Frame (DF) (1)
4 (15)	RBS w/ Doubler Pl. (5); RBS w/o Doubler Pl. (1); WUF-W (8) SidePlate® (1)	High (2); Low (13);	W14 (15)	35' bay width (1); 25' bay width (1); Pin-base condition (1); Welded beam-column @ DF (1); 22' first story height (2);

				Low damping constants (1); High damping constants (1); Alternating damping constants (1);
8 (5)	RBS w/ Doubler Pl. (3); RBS w/o Doubler Pl. (1); WUF-W (1)	High (0); Low (5);	W14 (4); W27(1)	Welded beam-column @ DF (1)
12 (20)	RBS w/ Doubler Pl. (17); RBS w/o Doubler Pl. (1); WUF-W (1) SidePlate® (1)	High (2); Low (18);	W14 (11); W27 (7); W36 (2);	20' Damper Bay Width (1); 35' bay width (1); 25' bay width (1); 22' first story height (2); Welded beam-column @ DF (1); Low damping constants (1); High damping constants (1); Alternating damping constants (1); Weak-axis col. orientation @ DF (1)
20 (6)	RBS w/ Doubler Pl. (3); RBS w/o Doubler Pl. (1); WUF-W (2)	High (0); Low (6);	W14 (2); W36 (4)	Welded beam-column @ DF (1); Weak-axis col. orientation @ DF (2)

* High gravity refers to a space frame configuration where moment frame columns carry significant gravity load; Low gravity refers to perimeter frame configurations where moment frame columns have relatively low gravity load compared to seismic load.

Analysis

Nonlinear models were developed using the *OpenSees* analysis platform (McKenna et al., 2010). Models are developed and analyzed assuming a representative 2D planar structure, with underlying moment frame (MF) designs neglecting the effects of biaxial loading and accidental torsion, to be consistent with the modeling procedures outlined in FEMA P-695.

Modeling of the MF sub-system follows the ATC-114/NIST nonlinear modeling guidelines (NIST, 2017) and includes recent research published following the release of the ATC-114/NIST guidelines. The MF models include three sources of nonlinearity: beam-to-column connections, column hinging, and panel zones. Relationships used to estimate the nonlinear behavior are based on regression analysis of experimental testing (Lignos and Krawinkler, 2011; Lignos et al., 2019; Skiadopoulos et al., 2021). Beam-to-column connection and column hinges include hysteretic energy-based degradation using the *BiLin* material in *OpenSees* (Ibarra et al., 2005).

Dampers are modeled using a Maxwell model approach, where the assembly stiffness of the damper (K_{TD}) is considered in series with the extender brace stiffness (K_E). An illustration of the Maxwell model is shown in Figure 3. The damper model uses a combination of a *truss* element with a *Viscous* material in series with an *elasticBeamColumn* element that provides the assembly stiffness (see K_A in Figure 3) and the viscous damping properties (C and α in Figure 3). All dampers assume a velocity exponent (α) of 0.4 per ICC-ESR 4769.

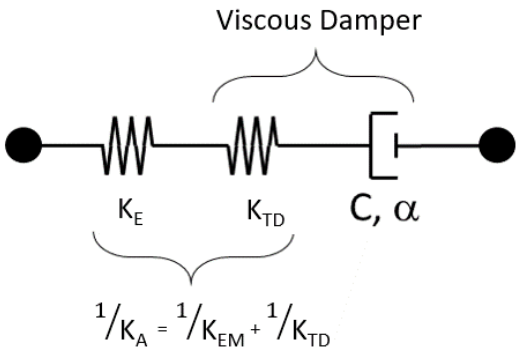

Figure 3. Maxwell model used for modeling nonlinear viscous dampers

The basic model configuration for a Type I system with a single-bay chevron damper frame (DF) configuration is shown in Figure 4. A Type I system does not have shared elements between the DF and the MF (ICC-ES, 2023). The moment frame (MF) is connected to the DF using rigid link *truss* elements. Similarly, a leaning P-Δ column is placed on the opposite side of the MF in order to capture gravity load effects from loads that are not tributary to the MF or DF. Typical modeling assumptions for Type I systems treats the DF column bases and beam connections as pinned, neglecting any strength or stiffness provided by these connections (see Figure 4). Inherent damping of the structure is modeled as 2% Rayleigh damping applied at the first and third mode periods (second mode for 2-story archetypes). Stiffness proportional Rayleigh damping is only applied to linear elastic elements, and the implemented formulation in *OpenSees* follows the recommendations of Zareian and Medina (2010) for lumped plasticity models.

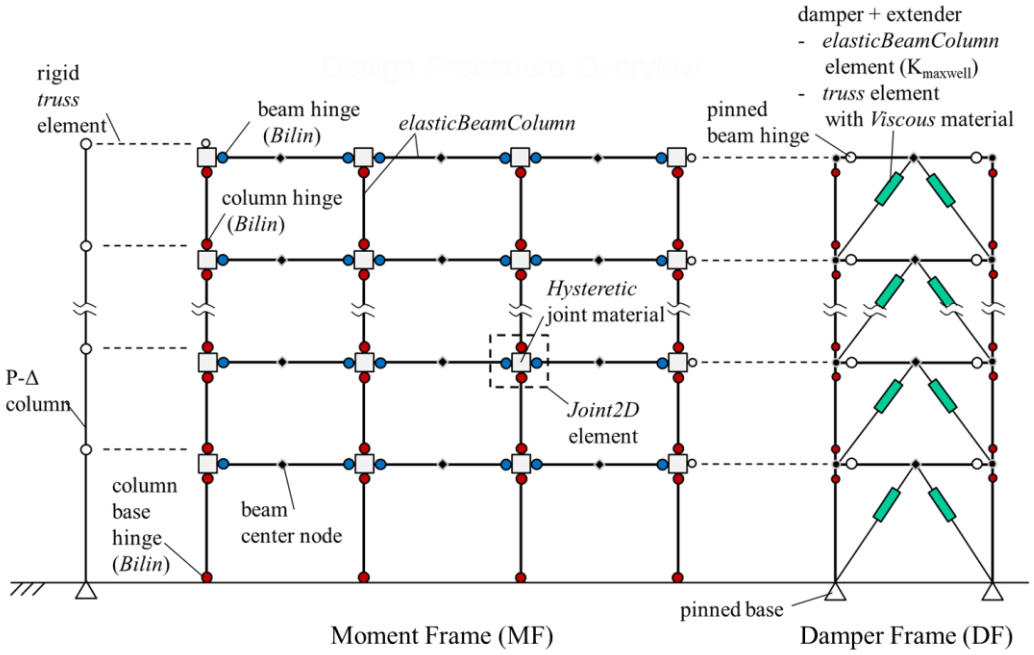

Figure 4. Nonlinear numerical model for a Type I TDMF™ system

The FEMA P-695 far-field ground motion record set (FEMA, 2009) was used as input for the nonlinear models. The ground motions consist of 22 horizontal pairs (44 individual accelerograms). Ground motions were scaled to the DE intensity (S_{DS} = 1.0g, S_{D1} = 0.6g) at the code-based period ($T = C_u T_a$) and 5% damping, per FEMA P-695.

Damper-Induced Diaphragm Forces

If structures behaved in a purely first-mode manner, where each floor was moving in the same direction at the same time during an earthquake and dampers experienced peak velocity (and therefore force) at the same time up the height of the building, then the damper-induced diaphragm force would simply be the difference between the peak damper force above and below the diaphragm of interest. This is, of course, not the case. What we observed from the step-by-step evaluation of the damper force above and below a given floor is that nonlinearity and higher mode effects cause instances where the velocity is acting in opposite directions at the floors above and below a given diaphragm. While this doesn't occur at the peak damper force, it does seem to occur at moments where the additive damper forces can approach the peak force from the damper above or below. Figure 5 shows one such time history for an 8-story RBS moment frame at the 4th fourth floor diaphragm. The following components are provided: a) the corresponding time history of horizontal components of the DE level damper forces above and below; b) the time history of the summation of the two damper forces, taking into account directionality; and c) the story drift ratio time history. The reaction force in Figure 5b would be the damper-induced diaphragm forces for this archetype structure, at this diaphragm level (the 4th floor) for this specific ground record.

In this example, the peak damper force above and below would be 221 and 238 kips, respectively, and the maximum damper-induced diaphragm force would also be just over 210 kips. It is worth noting that the peak damper forces occur near the same time in the record, but not at exactly the same moment, and are out of phase (see Figure 5a). Additionally, the moment of peak damper-induced diaphragm force takes place in a small window when the damper velocities are opposite above and below, therefore causing the damper forces to be additive. This condition, where the damper forces are additive, is not common throughout the time history, but did occur in each ground record examined and drives the derivation of the damper-induced diaphragm forces. Figure 5c demonstrates that the peak damper-induced reaction does not occur simultaneously with peak story drift demand, representing the largest shear reactions in the moment frame. This is important when considering how to combine the damper-induced diaphragm forces with the diaphragm inertial forces.

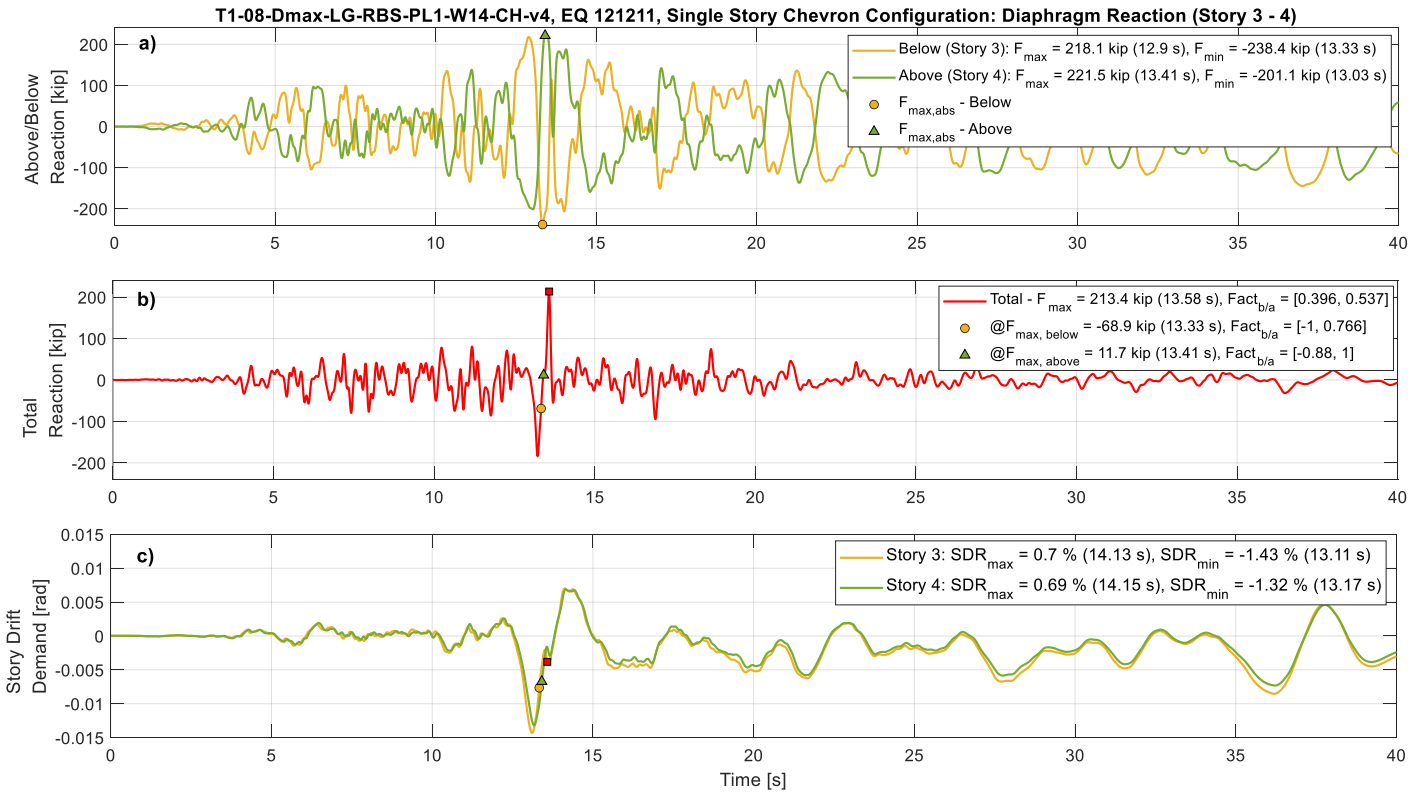

Figure 5. a) horizontal damper force reaction time history for the dampers above (green) and below (yellow) the diaphragm; b) total damper-induced diaphragm reaction time history; and c) story drift ratio time history.

Using this approach, the peak reaction force, or damper-induced diaphragm force, for each floor and each ground record was determined. Figure 6 shows the ratio of the peak reaction force to the largest DE level damper force for the floor above and below the diaphragm of interest, for each floor in the same 8-story RBS building and for each of the 44 ground records (gray circles). The average ratio and average plus one standard deviation across the 44 ground motions are shown.

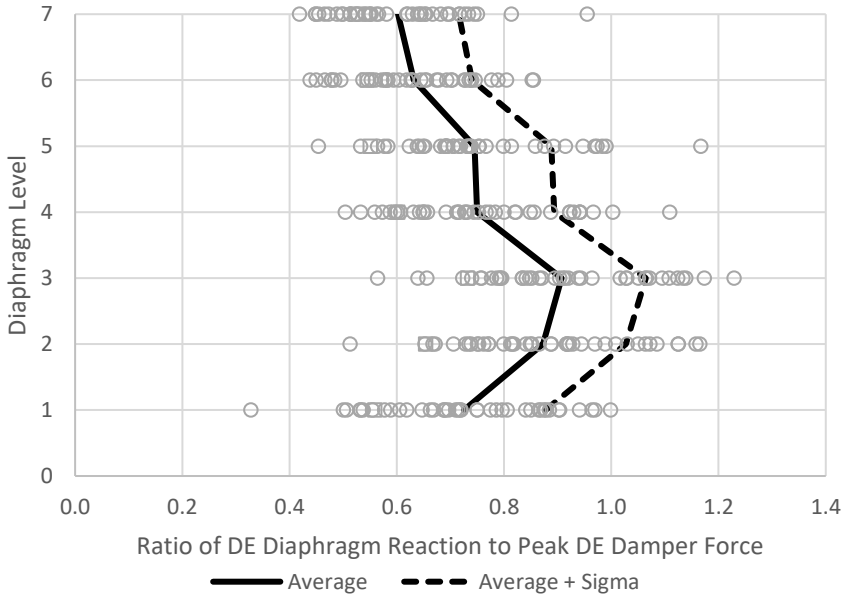

Figure 6. Ratio of peak reaction force to peak DE level damper force at each story and for each of 44 ground records for an 8-Story RBS archetype structure (T1-08-Dmax-LG-RBS-PL1-W14-CH-v4).

The average ratio (across the 44 ground records) of peak reaction force to peak DE level damper force for each of the five 8-story archetype structures is shown in Figure 7. The average across the archetypes in this performance group is shown in black. The average ratios for the peak reaction seen through the archetype study to a function of the damper forces is what was used to develop a generalized equation. This relationship was examined for each archetype structure individually, but also for each performance group using the average of the averages across archetype structures with the same number of stories. This process led to a generalized equation shown in the next section, dependent upon the number of stories and the DE level damper force above and below the diaphragm of interest. Similar results are provided for the 2, 4, 12 and 20-story archetype groups in Figure 8 through Figure 11.

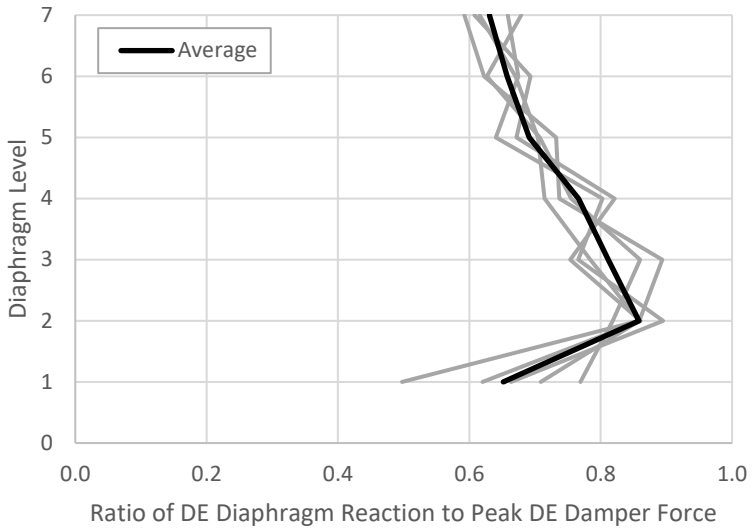

Figure 7. Average ratio of peak reaction force to peak DE level damper force for each of five (5) 8-story archetype structures at each story

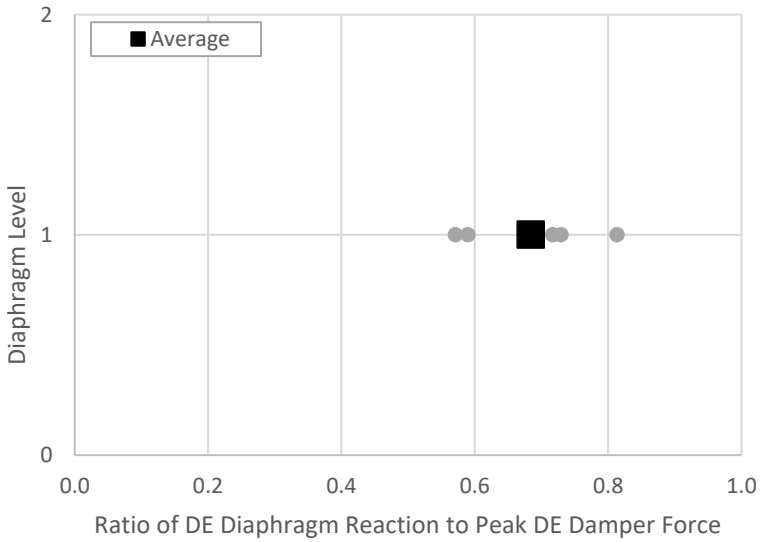

Figure 8. Average ratio of peak reaction force to peak DE level damper force for each of five (5) 2-story archetype structures at each story

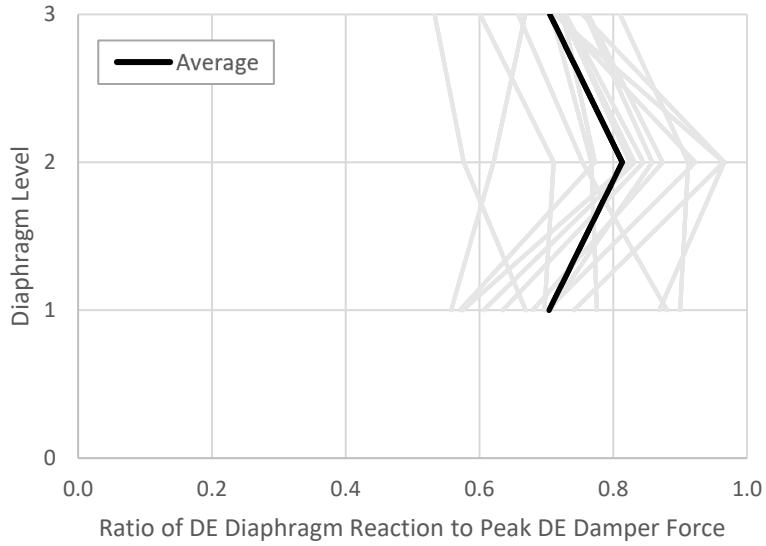

Figure 9. Average ratio of peak reaction force to peak DE level damper force for each of fifteen (15) 4-story archetype structures at each story

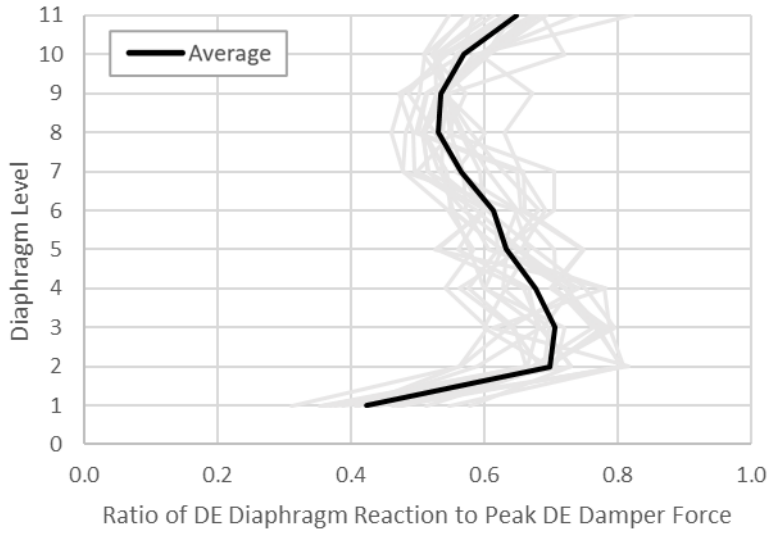

Figure 10. Average ratio of peak reaction force to peak DE level damper force for each of twenty (20) 12-story archetype structures at each story

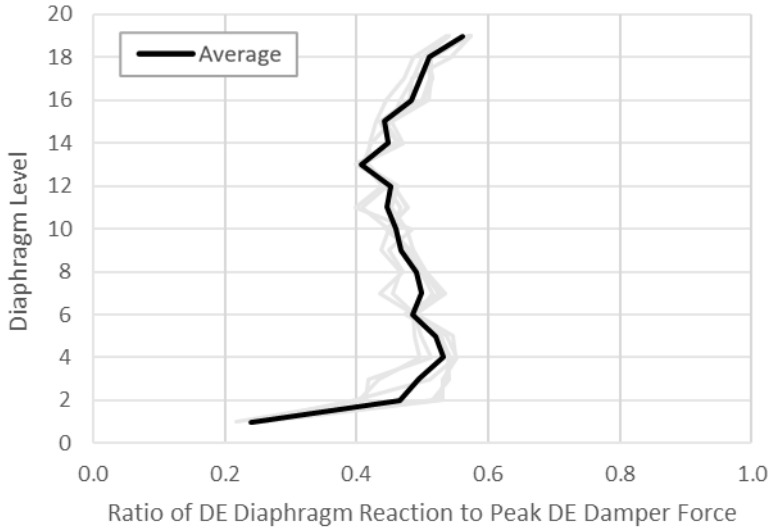

Figure 11. Average ratio of peak reaction force to peak DE level damper force for each of six (6) 20-story archetype structures at each story

Generalized Equation for Damper-Induced Forces into Diaphragms

The process shown above was conducted for each of the 51 archetype structures, for each of the 44 ground records and at each floor, creating a database of maximum DE damper forces above and below each floor as well as the maximum reaction. These data were distilled down to influence the derivation of a generalized equation for damper-induced forces in a diaphragm for use in linear methods. The objective was to develop an equation that would, as closely as reasonable, replicate the maximum reactions based on the DE level damper forces above and below the diaphragm of interest. In this tuning process, the maximum reaction force averaged across the 44 ground records for each archetype structure was used. Overstrength damper forces, rather than DE level forces, would be used in the generalized formula to account for dispersion in the reaction forces across the 44 records and across different archetype structures.

Based on the results, the following equation is proposed to capture the damper-induced forces in the diaphragm, $F_{px,FVD}$, when using linear methods:

$$F_{px,FVD} = (0.5 - 0.01 * n_s) * \left[\sum_{j=1}^{n_i}(F_{ji}) + \sum_{j=1}^{n_{i-1}}(F_{j(i-1)})\right] \quad \text{(Eqn. 2)}$$

Where,

$F_{px,FVD}$ = cumulative damper-induced diaphragm force at the ith story
n_s = number of above grade damped moment frame stories
n_i = total number of dampers in the direction of interest in the ith story, above the diaphragm of interest
n_{i-1} = total number of dampers in the direction of interest in the (i-1)th story, below the diaphragm of interest
F_{ji} = overstrength force in the jth damper in the ith story, above the diaphragm of interest
$F_{j(i-1)}$ = overstrength force in the jth damper in the (i-1)th story, below the diaphragm of interest

For each archetype structure, the ratio of the average peak reaction force to the generalized equation using DE level damper forces (instead of overstrength forces) was examined at each floor. This ratio was then averaged across each archetype structure for a given height (number of stories). The plot of these average ratios is shown at each story in Figure 12. A perfect match for the generalized equation would provide a vertical line at 1.0, demonstrating that the generalized

equation matched average reaction forces across the archetypes. A ratio less than 1.0 is conservative, meaning that the generalized equation predicts higher diaphragm forces than the average of the analysis showed.

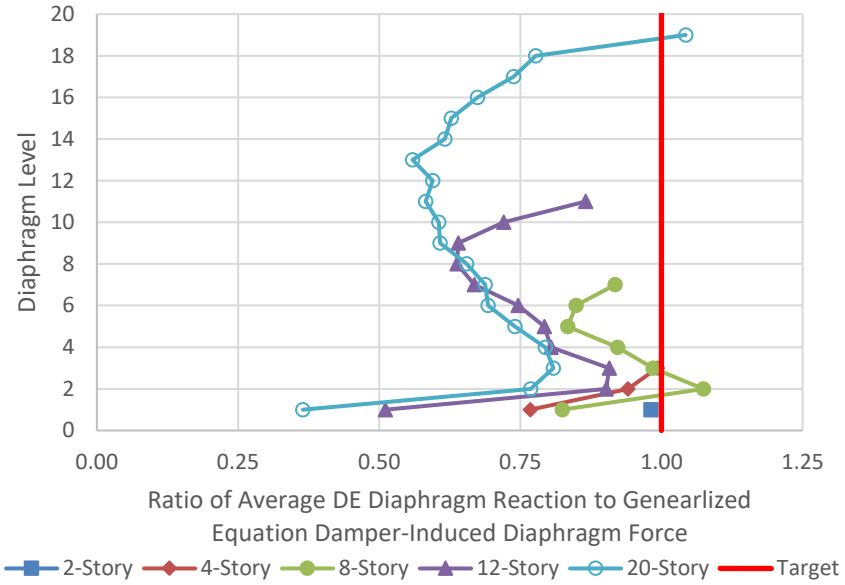

Figure 12. Ratio of Average Damper-induced Reaction Force from Analysis to Generalized Equation using DE level damper forces at each story

In developing a generalized equation, there is a challenging balance between simplicity and precision. The proposed generalized equation is relatively simple, relying only on the number of stories and the summation of the damper forces above and below. It is slightly conservative, especially for middle stories of taller structures. It also gains further conservatism by ultimately using the overstrength damper force (1.66 times the DE level force). It was felt that the conservatism was warranted in this case, however, given the spread of damper-induced diaphragm reactions seen across the suite of ground records and the effects of reducing responses from velocity-based devices to a linear analysis. For these reasons, the proposed generalized equation was a good fit for code-based design efforts when using linear methods for damped-moment frames.

It is worth noting that the proposed equation uses the summation of the damper forces above and below, rather than attempting to develop an equation based on individual dampers. While the archetype structures have the same number of dampers above and below, and the dampers are stacked in the same damper frame up the full height of the building, this is often not the case in real buildings. Dampers are oftentimes not stacked in a single bay – an advantage of FVDs not contributing stiffness to the system – and there are often more dampers in lower stories than in upper stories. To avoid the complexity of these conditions, the summation of all the horizontal damper force above and below, in the principal direction under consideration, is used. The resulting damper-induced diaphragm force would be equally distributed across the diaphragm, similar to how inertial forces are distributed. This is not so say that local load effects must not be considered; there still remains the need for a complete load path from the damper generated force through connecting elements and into the diaphragm.

Finally, this damper-induced diaphragm force needs to be combined with inertial diaphragm forces caused by the acceleration of the diaphragm mass. There are several important considerations with this combining:

- The presence of dampers in the building reduces floor accelerations and therefore diaphragm inertial forces. The TDMF™ procedure allows for the bounds on the diaphragm inertial forces (ASCE 7-22 Equations 12.10-2, 12.10-

3 and 12.10-5) to be reduced by 25%. Table 18.7-1 could similarly be used to determine this reduction when the linear methods of ASCE 7-22 are used.

- FVDs are velocity-based devices and therefore peak out-of-phase with inertial forces. It is recommended to use the prescribed load combinations from the ICC-ESR 4769, with 100% of the inertial forces combining with 70% of the damper-induced diaphragm forces and vis a versa. This is also supported by the theoretical derivations provided in Section 4.8 of Ramirez et al. (2001).
- The combination of damper-induced diaphragm forces with inertial forces should apply only to the internal forces for the diaphragm (shear and flexure/chords). This lateral load caused by the dampers is not carried further into the Moment Frames as an added story shear.
- At conditions where the dampers are in-line or within the Moment Frames, the damper-induced diaphragm force should be ignored. The load path of the damper forces should be through drag lines back to the moment frame but not added as an additional lateral load to the Moment Frames – this is already accounted for in the force-reduction factor, R, and base shear determination.
- Irrespective of the damper location in relation to the Moment Frame, a complete load path from the damper, into connections, gusset plate, column, beam and diaphragm is necessary. This local load path utilizes the maximum overstrength damper force.
- At floors with dampers only on one of the two adjacent stories, the full horizontal damper force would need to be resolved into the diaphragm.

Conclusions

This study attempts to fill a gap in the literature regarding the damper-induced diaphragm forces associated with the design of steel moment frames with supplemental fluid dampers using linear design methods. Recently developed linear methods based on Modal Response Spectrum Analysis are making it easier to implement fluid viscous dampers into structures, but the dynamic interaction between diaphragm inertial demands and velocity-based damper induced demands is lost. This study used an archetype design space consisting of 51 structures designed using the Taylor Damped Moment Frame procedure and analyzed with nonlinear time history to develop a generalized equation for use in code-based designs. This generalized equation contains layers of conservatism that are appropriate for the reduction of a nonlinear and highly dynamic system into a linear dynamic approach. Further research could continue the validation of this generalized equation, comparing the results from section cuts in a three-dimensional nonlinear time history to the demands from this prescriptive approach.

References

ASCE/SEI (American Society of Civil Engineering), 2022, *Minimum Design Loads and Associated Criteria for Buildings and Other Structures (ASCE 7-22)*. Reston, VA: ASCE

FEMA (Federal Emergency Management Agency), 2009, *Quantification of Building System Performance Factors (FEMA P695)*. Washington, DC: FEMA

Ibarra, L. F., Medina, R. A., and Krawinkler, H., "Hysteretic models that incorporate strength and stiffness deterioration," *Earthquake Engineering and Structural Dynamics*, 2005, Vol. 34, No. 12, pp. 1489-1511, John Wiley & Sons, Inc.

ICC-ES, 2019, "Acceptance Criteria for Qualification of Building Seismic Performance of Alternative Seismic Force-Resisting Systems (ICC-ES Guidance Document to FEMA P695)", AC494, and Annex C "Steel Moment Frames with Supplemental Viscous Damper Frames", 2022. International Code Council Evaluation Service, Brea, California.

ICC-ES, 2023, “Taylor Damped Moment Frame System (TDMF™),” *ICC-ES Evaluation Report ESR-4769*. International Code Council Evaluation Service, Brea, California.

Lignos, D. G., and Krawinkler, H., “Deterioration Modeling of Steel Components in Support of Collapse Prediction of Steel Moment Frames under Earthquake Loading,” *Journal of Structural Engineering*, 2011, Vol. 137, No. 11, pp. 1291-1302, American Society of Civil Engineers, Reston, Virginia.

Lignos, D. G., Hartloper, A. R., Elkady, A., Deierlein, G. G., and Hamburger, R., “Proposed Updates to ASCE 41 Nonlinear Modeling Parameters for Wide-Flange Steel Columns in Support of Performance-Based Seismic Engineering,” *Journal of Structural Engineering*, 2019, Vol. 145, No. 9, American Society of Civil Engineers, Reston, Virginia.

McKenna, F., Scott, M. H., and Fenves, G. L., “Nonlinear finite-element analysis software architecture using object composition,” *Journal of Computing in Civil Engineering*, 2010, Vol. 24, No. 1, pp. 95-107, American Society of Civil Engineers, Reston, Virginia.

NIST, 2017, *Recommended Modeling Parameters and Acceptance Criteria for Nonlinear Analysis in Support of Seismic Evaluation, Retrofit and Design*, Report NIST GCR 17-917-45, Prepared by the Applied Technology Council for the National Institute of Standards and Technology (NIST), Gaithersburg, MD.

Ramirez, O. M., Constantinou, M. C., Kircher, C. A., Whittaker, A. S., Johnson, M. W., Gomez, J. D., and Chrysostomou, C. Z., 2001, *Development and Evaluation of Simplified Procedures for Analysis and Design of Buildings with Passive Energy Dissipation Systems*, MCEER Report 00-0010, Revision, 1, Multidisciplinary Center for Earthquake Engineering Research, University at Buffalo, State University of New York, Buffalo, NY, 470 pp.

Skiadopoulos, A., Elkady, A., and Lignos, D. G., “Proposed Panel Zone Model for Seismic Design of Steel Moment-Resisting Frames,” *Journal of Structural Engineering*, 2021, Vol. 147, No. 4, American Society of Civil Engineers, Reston, Virginia.

Vamvatsikos, D., and C. A. Cornell, "Incremental dynamic analysis," *Earthquake Engineering and Structural Dynamics*, 2002, Vol. 31, No. 3, pp. 491-514, John Wiley & Sons, Inc.

Welch, D. P., DeBock, D. J., Canney, N. E., and Harris, J. R., “Practical design procedure for steel moment frames with fluid viscous dampers,” *2022 SEAOC Convention*, August 31-September 3, 2022, Indian Wells, CA.

Zareian, F., and Medina, R. A., “A practical method for proper modeling of structural damping in inelastic plane structural systems,” *Computers and Structures*, 2010, Vol. 88, No. 1, pp. 45-53, Elsevier.